RSC Advances

PAPER

Cite this: *RSC Adv.*, 2021, **11**, 23802

Solubility, thermal and photoluminescence properties of triphenyl imidazole-containing polyimides†

Wu Bai,[a] Zhizhi Hu,*[ab] Yunhua Lu,*[a] Guoyong Xiao,[a] Hongbin Zhao,[ab] Jianmin Zhu[b] and Zhaobin Liu[b]

In this paper, three kinds of triphenyl imidazole-containing diamines including 2-phenyl-4,5-bis(4-(4-amino-2-trifluoromethylphenoxy)phenyl)imidazole (PBAI), 2-(4-methylphenyl)-4,5-bis(4-(4-amino-2-trifluoromethyl phenoxy)phenyl)imidazole (MPBAI) and 2-(4-trifluoromethylphenyl)-4,5-bis(4-(4-amino-2-trifluoromethylphenoxy)phenyl)imidazole (TFPBAI) were synthesized. Then, a series of polyimide (PI) films were prepared by the solution polymerization of the three diamines and various dianhydrides, such as 4,4′-(hexafluoroisopropylidene)diphthalic anhydride (6FDA), 1,2,4,5-pyromellitic dianhydride (PMDA) and 1,2,3,4-cyclobutanetetracarboxylic dianhydride (CBDA), followed by thermal imidization. The effects of chemical structures on the solubilities and thermal, optical and electrochemical properties of polyimides were explored. All the polyimides exhibited higher glass transition temperatures around 300 °C and excellent solubilities in common polar solvents. The polyimide films derived from CBDA or 6FDA showed better optical properties with light color and transparent characteristics. The fluorescence test showed that the photoluminescence color of CBDA-based polyimide films is in the blue range in the CIE 1931 spectrum, while the polyimide film based on PMDA and 6FDA presented black or weak yellow light. However, all these polyimides in solution exhibited similar blue luminescence. Electrochemical tests indicated that the HOMO and LUMO values of these films were around −6.5 and −3.6 eV, and the energy gap difference was about 3.0 eV. Therefore, the triphenyl imidazole-containing polyimides exhibit comprehensive performance, which will be expected as a new kind of functional material for certain application in the optical and optoelectronics fields.

Received 9th April 2021
Accepted 30th June 2021

DOI: 10.1039/d1ra02765d

rsc.li/rsc-advances

1. Introduction

Aromatic polyimides (PIs), as a kind of high-performance engineering material, have attracted wide attention because of their excellent properties, such as chemical solvent resistance, excellent thermal and mechanical properties, and outstanding dielectric performance, and they have been widely used in the fields of microelectronics, separation membranes, aerospace and other applications.[1–4] The traditional aromatic polyimides display a brown-yellow color. The reason is mainly that the charge transfer complex (CTC) is easily formed between the electron donor (diamine) and electron acceptor (dianhydride), resulting in the absorption of light. The idea was firstly proposed by Dine-Hart in 1971 and well discussed by Kotov in 1977.[5,6] Hence, the polyimide films are greatly limited in optical applications.[5–9] Besides, due to strong interaction between molecular chains, most polyimides are insoluble in common solvents, leading to poor processability.[8] In order to solve these problems, many researchers and engineers have made considerable efforts in recent years. Some strategies have been proposed, including introduction of unsymmetrical structure and flexible linkage, incorporation of large volume pendant substituents, addition of alicyclic unit and copolymerization, to hinder the formation of CTC.[10–14] The highly transparent fluorinated PIs were firstly invented by Dupont in 1961, followed by detailed studies by NASA and St. Clair in 1980's.[7–9] Now, the introduction of $-CF_3$ groups are commonly adopted to increase the solubility and optical transparency of the polyimides because of their weak electronic polarization and high electronegativity as well as bulky steric hindrance.[15–17]

Aryl imidazole is a large volume structure with imidazole as the center, which has attracted people's interest due to its photosensitive properties.[18–20] As well known, small molecule luminescent materials are widely used in planar display, fluorescent sensing, biological imaging and other fields.[21–24] Now, polymer luminescent materials are expected to be functional materials as flexible devices, anti-counterfeiting and sun protection coatings because of their good processability and film-

[a]School of Chemical Engineering, University of Science and Technology Liaoning, Anshan, Liaoning, P. R. China. E-mail: huzhizhi@163.com; lee.lyh@163.com
[b]Oxiranchem Holding Group Co. Ltd., Liaoyang, Liaoning, P. R. China

† Electronic supplementary information (ESI) available. See DOI: 10.1039/d1ra02765d

forming properties.[25–27] The basic design and theory of fluorescent polyimides were firstly established by Wakita in 2009.[28] Recently, aryl imidazole structures, including triaryl imidazole and tetraaryl imidazole have been introduced into polyimide side chains, which greatly improve the solubility and thermal properties of polyimides.[29–38] The rigid, bulky and thermally stable aryl imidazole moiety could reduce close packing, increase the chain distance, leading to irregular arrangement, which is conductive to the solvent to pass through.[39–41] Moreover, large volume heterocyclic rings is helpful to improve or maintain the thermal stabilities of polyimides.[38,39] However, the fluorescence quantum yield of aromatic polyimides is very low, which could not meet the needs of practical application.[42,43] The conjugation of aromatic polyimide backbones and intramolecular or intermolecular charge transfer (CT) transition significantly cause fluorescence to be weakened or quenched.[44–46] Therefore, polyimide solution is often reported to emit blue fluorescence, while the film emits no fluorescence or only weak fluorescence, which hinders its optical application. In order to avoid fluorescence quenching, several methods are presented, such as the introduction of alicyclic structures, flexible linkage and large volume substituents, which are conductive to reduce the effect of charge transfer in the polymers.[44–48]

In this paper, the triphenylimidazole structure is introduced into three diamines, and then polymerized with three commercially available dianhydrides to synthesize polyamic acid solutions. Then, polyimide films containing triphenylimidazole were prepared by thermal imidization, and the influence of the chemical structure on the thermal properties, solubility, and optical properties was studied in detail. These polyimides exhibited excellent solubility and thermal properties, and the polyimide films derived from alicyclic structures obviously showed photoluminescence behavior. Therefore, the polyimide materials containing triphenylimidazole are expected to be used in the fields of flexible light-emitting devices, fluorescent sensors, plastic lasers, solar cells, and light wave converters in the future.

2. Experimental

2.1 Materials

4,4′-Dihydroxydiphenyl ethylenedione, benzaldehyde, *p*-methylbenzaldehyde, *p*-trifluoromethylbenzaldehyde, and 2-chloro-5-nitrobenzotrifluoride were purchased from Shanghai Aladdin Biochemical Technology Co., Ltd. (China) and used directly without purification. 4,4′-(Hexafluoroisopropylidene) diphthalic anhydride (6FDA) and 1,2,4,5-pyromellitic dianhydride (PMDA) were bought from Chinatech Chemical Co., Ltd. (China) and 1,2,3,4-cyclobutanetetracarboxylic dianhydride (CBDA) was provided by Oxiranchem Holding Group Co. Ltd. (China). All other reagents were obtained from Sinopharm Chemical Reagent Co., Ltd. (China) and used as received.

2.2 Synthesis of diamines

The synthesis steps of triphenyl imidazole-containing diamines are shown in Scheme 1. The chemical structures were identified by FTIR and ^{1}H NMR, as shown in Fig. S1 and S2.†

Synthesis of 4,4′-(4-nitro-2-trifluoromethylphenoxy)diphenylethylenedione (BNTFPED). 48.446 g (0.200 mol) 4,4′-dihydroxydiphenyl ethylenedione, 91.122 g (0.404 mol) 2-chloro-5-nitrobenzotrifluoride and 150 mL dimethyl sulfoxide (DMSO) were added to a 500 mL two-necked flask and kept stirring at room temperature. Then, 33.940 g (0.404 mol) sodium bicarbonate ($NaHCO_3$) was introduced into the solution and heated to 100 °C. The reaction was tracked by liquid chromatography (HPLC) for 6 h, and then the brown reaction solution was cooled to room temperature and slowly poured into deionized water of 1 L while stirring. A large amount of light yellow solid was precipitated, and the filter cake was washed with water repeatedly. After drying, the crude product of 120.500 g was obtained, which was further recrystallized by ethylene glycol methyl ether to obtain light yellow fine needle-like crystals. The yield was about 90.0%, and the relative content (HPLC) was greater than 99.0%. Melting point: 188.9–191.1 °C. ^{1}H NMR (500 MHz, DMSO-d_6, ppm): δ: 8.58 (s, 2H), 8.54 (d, J = 9.3 Hz, 2H), 8.09 (d, J = 8.2 Hz, 4H), 7.44 (t, J = 9.9 Hz, 6H). FTIR (KBr, cm^{-1}): 1668 (C=O), 1582, 1362 (NO_2), 1112 (C–O–C).

Synthesis of 2-phenyl-4,5-bis(4-(4-nitro-2-trifluoromethylphenoxy)phenyl)imidazole (PBNI). 9.310 g (0.015 mol) of BNTFPED, 1.600 g (0.015 mol) of benzaldehyde, 11.560 g (0.150 mol) of ammonium acetate (CH_3COONH_4) and 40 mL of glacial acetic acid (CH_3COOH) were put into a 150 mL two-necked flask. The reaction was heated to 120 °C and refluxed for 8–10 hours. Then, the yellow reaction solution was cooled to room temperature and slowly poured into 250 mL of deionized water. The yellow solid was subsided, and the filter cake was washed with water several times until the filtrate was nearly colorless. After the dried crude product was further purified by ethylene glycol methyl ether, the yellow crystals were attained with a yield of 80% and relative content of 99.8% (HPLC). Melting point: 136.6–137.9 °C. ^{1}H NMR (500 MHz, DMSO-d_6, ppm): δ: 12.83 (s, 1H), 8.58–8.50 (m, 3H), 8.48 (d, J = 9.4 Hz, 1H), 8.10 (d, J = 7.7 Hz, 2H), 7.71 (dd, J = 18.7, 7.8 Hz, 4H), 7.50 (t, J = 7.5 Hz, 2H), 7.44–7.33 (m, 3H), 7.27–7.14 (m, 4H). FTIR (KBr, cm^{-1}): 1526, 1350 (NO_2), 3412 (N–H), 1131 (C–O–C).

Synthesis of 2-phenyl-4,5-bis(4-(4-amino-2-trifluoromethylphenoxy)phenyl)imidazole (PBAI). PBNI of 7.060 g (0.01 mol), palladium carbon (10% Pd) of 0.500 g and absolute ethanol of 50 mL were put into a 100 mL two-necked flask. After the reaction solution was heated to 70 °C, 7 mL of hydrazine hydrate (85%) was slowly dripped and stirred for 6 h. Before the reaction solution was cooled to room temperature, the palladium carbon catalyst was filtered hot and removed. Then, the solid–liquid mixture was obtained by rotary evaporation of the filtrate under reduced pressure to remove most solvents. After filtration, the filter cake was rinsed by a small amount of deionized water. Finally, the dried product of 5.900 g was obtained with a yield of 70% and a HPLC purity of 99.7%. Melting point: 104.7–105.6 °C. ^{1}H NMR (500 MHz, DMSO-d_6, ppm): δ: 12.60 (s, 1H), 8.05 (d, J = 7.8 Hz, 2H), 7.52 (d, J = 7.7 Hz, 2H), 7.46 (t, J = 6.6 Hz, 4H), 7.36 (t, J = 7.3 Hz, 1H), 7.01–6.89 (m, 6H), 6.84 (t, J = 11.1 Hz, 4H), 5.50 (d, J = 28.0 Hz, 4H). FTIR (KBr, cm^{-1}): 3360, 1628 (N–H), 1618 (C=N), 1336 (C–N), 1117 (C–O–C).

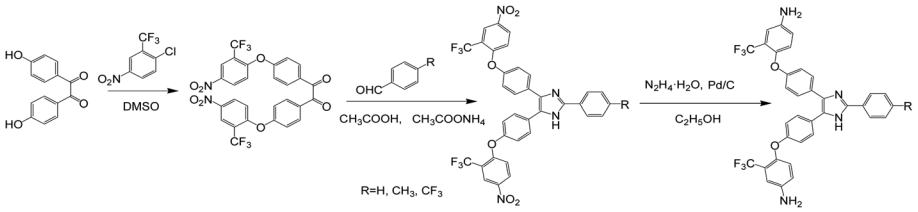

Scheme 1 Synthesis routes of the intermediate BNTFPED, PBNI, MPBNI, TFPBNI and the diamine PBAI, MPBAI, TFPBAI.

According to similar method, other dinitro compounds and diamines were also synthesized. 2-(4′-Methylphenyl)-4,5-bis(4-(4-nitro-2-trifluoromethylphenoxy)phenyl)imidazole (MPBNI): orange-yellow crystal, HPLC relative content of 99.9%. Melting point: 168.7–165.9 °C. ^{1}H NMR (500 MHz, DMSO-d_6, ppm): δ: 12.74 (s, 1H), 8.54 (d, J = 12.3 Hz, 3H), 8.48 (d, J = 9.4 Hz, 1H), 7.99 (d, J = 7.1 Hz, 2H), 7.70 (dd, J = 19.9, 6.8 Hz, 4H), 7.33 (dd, J = 23.9, 7.3 Hz, 4H), 7.26–7.13 (m, 4H), 2.37 (s, 3H). FTIR (KBr, cm^{-1}): 1530, 1329 (NO_2), 3089 (N–H), 1622 (C=N), 1329 (C–N), 1114 (C–O–C).

2-(4-Methylphenyl)-4,5-bis(4-(4-amino-2-trifluoromethylphenoxy)phenyl)imidazole (MPBAI). White powdery solid, HPLC relative content of 99.8%. Melting point: 125–125.9 °C. ^{1}H NMR (500 MHz, DMSO-d_6, ppm): δ: 12.50 (s, 1H), 7.94 (d, J = 6.1 Hz, 2H), 7.56–7.41 (m, 4H), 7.27 (d, J = 7.1 Hz, 2H), 6.94 (d, J = 8.7 Hz, 5H), 6.83 (d, J = 6.8 Hz, 4H), 5.49 (d, J = 27.4 Hz, 4H), 2.35 (s, 3H). FTIR (KBr, cm^{-1}): 3380, 1629 (N–H), 1611 (C=N), 1336 (C–N), 1119 (C–O–C).

2-(4-Trifluoromethylphenyl)-4,5-bis(4-(4-nitro-2-trifluoromethylphenoxy)phenyl)imidazole (TFPBNI). Light yellow crystal, HPLC relative purity of 99.9%. Melting point: 151.7–152.8 °C. ^{1}H NMR (500 MHz, DMSO-d_6, ppm): δ: 13.12 (s, 1H), 8.61–8.42 (m, 4H), 8.31 (s, 2H), 7.88 (s, 2H), 7.79–7.63 (m, 4H), 7.38 (s, 2H), 7.20 (dd, J = 17.4, 12.5 Hz, 4H). FTIR (KBr, cm^{-1}): 1530, 1323 (NO_2), 3093 (N–H), 1622 (C=N), 1323 (C–N), 1112 (C–O–C).

2-(4-Trifluoromethylphenyl)-4,5-bis(4-(4-amino-2-trifluoromethylphenoxy)phenyl)imidazole (TFPBAI). White powdery solid, HPLC relative content of 99.5%. Melting point: 117.0–118.9 °C. ^{1}H NMR (500 MHz, DMSO-d_6, δ, ppm): δ 12.90 (s, 1H), 8.26 (d, J = 7.6 Hz, 2H), 7.84 (d, J = 6.2 Hz, 2H), 7.50 (dd, J = 25.1, 7.3 Hz, 4H), 7.02–6.88 (m, 5H), 6.88–6.77 (m, 4H), 5.50 (d, J = 28.1 Hz, 4H). FTIR (KBr, cm^{-1}): 3370, 1619 (N–H), 1617 (C=N), 1324 (C–N), 1114 (C–O–C).

2.3 Preparation of polyimide films

The triphenyl imidazole-containing polyimide films were prepared according to the conventional two-step method, including the solution polymerization of diamines and dianhydrides as well as thermal imidization, as shown in Scheme 2. First, 1.940 g (0.003 mol) of diamine PBAI and 14.300 g solvent *N*,*N*-dimethylacetamide (DMAc) were added to a 100 mL round bottom flask and stirred for about 30 minutes. After the PBAI was completely dissolved, 0.594 g (0.003 mol) of dianhydride CBDA was introduced and continuously mixed at ambient temperature for 24 h. Then, the obtained poly(amic acid) (PAA) solution was coated on a clean glass substrate, followed by the temperature-programmed thermal imidization, which was as follows: 80 °C per 30 min, 120 °C per 30 min, 160 °C per 30 min, 200 °C per 30 min, 250 °C per 30 min and 300 °C per 20 min. After natural cooling, the glass plate was immersed into a water bath at 80 °C to remove the film. Finally, the obtained film was dried at 100 °C for the next test.

2.4 Characterization

The chemical shifts of the dinitro compounds and diamines were measured by AVANCE 500 MHz nuclear magnetic field

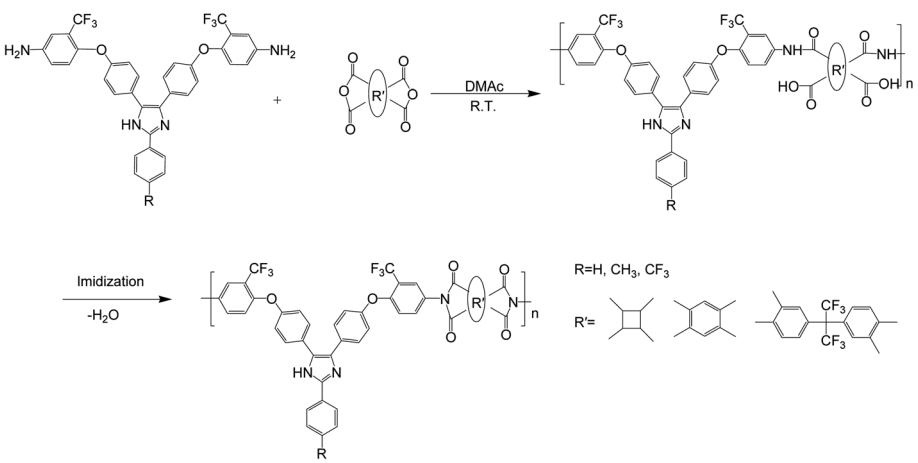

Scheme 2 Synthesis of triphenyl imidazole-containing polyimides.

resonator (Bruker, Swiss), and the deuterated reagent was dimethyl sulfoxide (DMSO). The characteristic functional groups of the compounds and polymers were tested by Nicolet IS10 Fourier infrared spectrometer (Thermo Fisher Scientific, USA) in the range of 500–4000 cm^{-1}. The BLKII-5FF-SX X-ray diffractometer (PANalytical, Netherlands) was adopted to study the crystallinity of the polyimides, with a scanning rate of 0.5° s^{-1} from 5° to 90°. The solubilities of polyimide films were explored by immersing 0.050 g film samples into glass tubes with various solvents of 1 mL for 24 h. Pyris 1 TGA thermal analyzer (PerkinElemer, USA) was used to investigate the thermal stabilities of the polyimides, with a heating rate of 20 °C min^{-1} and nitrogen flow rate of 20 mL min^{-1} in the range of 30–900 °C. Dynamic thermomechanical analyzer DMA 8000 was utilized to research the thermal properties at a heating rate of 5 °C min^{-1} from 50 to 400 °C under nitrogen atmosphere (PerkinElmer, USA). Based on the maximum tan δ peak, the glass transition temperature (T_g) of the polyimides was determined. The UV-visible absorption spectra of the film samples were tested by Lambda 900 UV/Vis/NIR spectrophotometer (PerkinElmer, USA), scanning from 250 to 800 nm. The fluorescence testing in solid films or solutions was conducted on LS55 fluorescence/phosphorescence/luminescence spectrophotometer (PerkinElmer, USA) in the range of 250–800 nm to obtain the fluorescence emission and excitation spectra. The fluorescence quantum yield was tested by HORIBA Fluorolog-3 fluorescence spectrometer with an integrating sphere (Jobin Yvon, USA). For the polyimide film and solution samples, barium sulfate and quinine sulfate (Φ_f = 0.54) were used as references, respectively. The electrochemical performance of polyimides in solution was studied by electrochemical workstation (IVIUM, Netherlands) in a three-electrode system with 0.1 M $Bu_4N(ClO_4)$ as the electrolyte in DMF at a scanning speed of 50 mV s^{-1}. The counter electrode was platinum wire, the working electrode was glassy carbon, and the reference electrode was Ag/AgCl. All the potentials were calibrated with ferrocene as an external standard.

3. Results and discussions

3.1 Chemical structures

The chemical structures of triphenyl imidazole-containing polyimides were identified by FTIR, as shown in Fig. 1. It can be seen that all polyimides exhibit characteristic peaks of imide ring, including 1785 cm^{-1} (the asymmetric stretching vibration peak of C=O group), 1715 cm^{-1} (the symmetric stretching vibration peak of C=O group) and 1372 cm^{-1} (the stretching vibration absorption of C–N bond). The peaks near 2800–3000 cm^{-1} belong to the N–H bond of imidazole ring. These characteristic peaks indicate that the triphenyl imidazole-containing polyimides have undergone a relatively complete imidization process.

3.2 X-ray diffraction analysis

The microstructures of triphenyl imidazole-containing polyimides were studied by XRD. As shown in Fig. 2, these X-ray diffraction peaks are mainly concentrated around 2Theta = 20.0°, and the calculated *d*-spacings are mostly about 0.44 nm

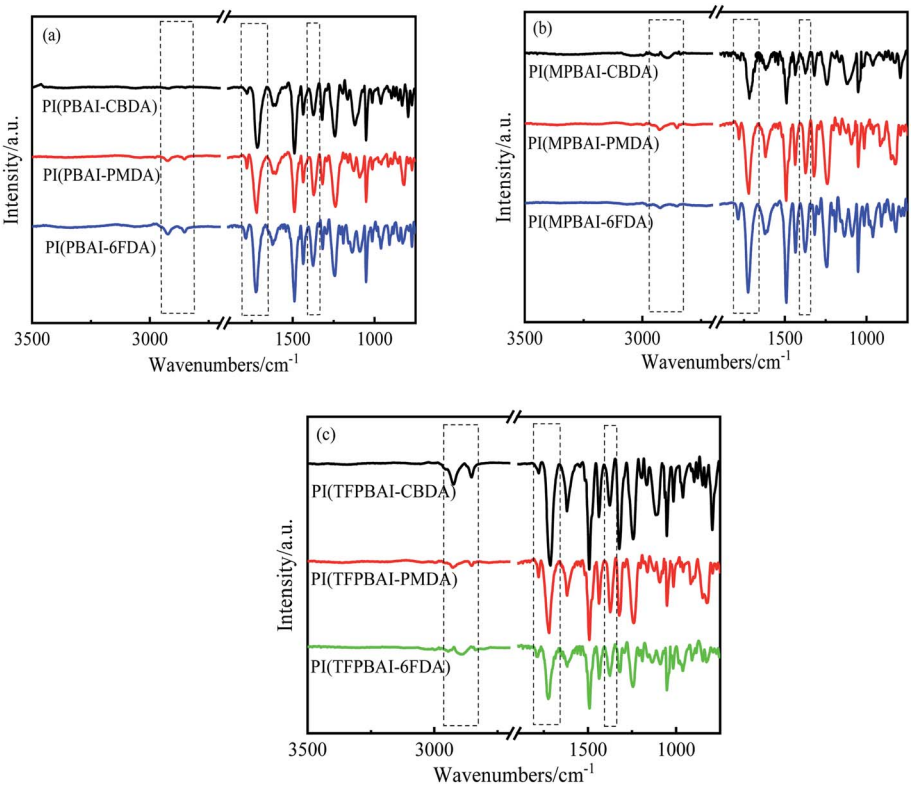

Fig. 1 FTIR spectra of triphenyl imidazole-containing polyimides (a) PIs based on PBAI, (b) PIs based on MPBAI, (c) PIs based on TFPBAI.

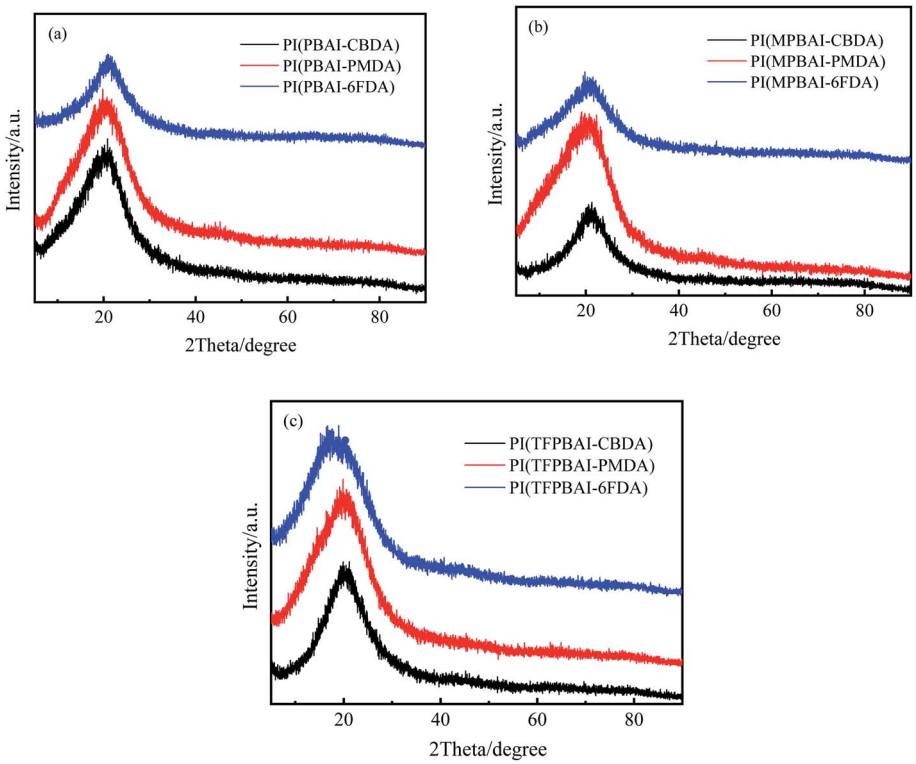

Fig. 2 XRD patterns of triphenyl imidazole-containing polyimides (a) PIs based on PBAI, (b) PIs based on MPBAI, (c) PIs based on TFPBAI.

according to the Bragg equation. Generally, these XRD curves show no remarkable sharp diffraction peaks, so the halo peaks mean amorphous characteristic of these polyimides. Additionally, the top of all the XRD curves is slightly sharp, which shows that the polymer chains form certain regular arrangements. In Fig. 2(c), the *d*-spacing of PI(TFPBAI-6FDA) reaches 0.51 nm (2Theta = 17.4°), which is attributed to the introduction of $-CF_3$ groups. The bulky structures of triphenyl imidazole and $-CF_3$ substituents increase the molecular chain distance, reduce the interaction between molecular chains, and weaken the order arrangement.[10–14]

3.3 Solubility

The solubilities of triphenyl imidazole-containing polyimides were tested in various solvents, including *N*-methylpyrrolidone (NMP), *N*,*N*-dimethylacetamide (DMAc), *N*,*N*-dimethylformamide (DMF), dimethyl sulfoxide (DMSO), sulfuric acid, acetone and chloroform, and the corresponding experimental results are given in Table 1. It is obvious that all the triphenyl imidazole-containing polyimides demonstrate excellent solubilities, which are soluble in common aprotic polar solvents, such as DMAc, DMF, NMP and DMSO. Furthermore, the polyimides derived from 6FDA show more excellent solubility than other polyimides, which could even be well dissolved in acetone. The reason may be that the bulky triphenylimidazole and $-CF_3$ groups increase the distance between molecular chains, twist the polymer main chain, reduce the molecular chain interactions, and create a large number of free volume, which are beneficial to the diffusion of solvents molecules.[15–17] Besides, the C–F bond exhibits lower polarizability, the solubilities of the polyimides in solvents could also be improved. Moreover, the flexible ether linkage enhances the

Table 1 Solubilities of triphenyl imidazole-containing polyimides[a]

Samples	NMP	DMAc	DMF	DMSO	Sulfuric acid	Acetone	Chloroform
PI(PBAI-CBDA)	++	++	++	++	+	+	-
PI(PBAI-PMDA)	++	++	++	++	+	+	- -
PI(PBAI-6FDA)	++	++	++	++	+	++	-
PI(MPBAI-CBDA)	++	++	++	++	+	+	-
PI(MPBAI-PMDA)	++	++	++	++	+	+	- -
PI(MPBAI-6FDA)	++	++	++	++	+	++	-
PI(TFPBAI-CBDA)	++	++	++	++	+	+	-
PI(TFPBAI-PMDA)	++	++	++	++	+	+	-
PI(TFPBAI-6FDA)	++	++	++	++	+	++	-

[a] ++: soluble at room temperature, +: soluble on heating, -: partially dissolved on heating, - -: insoluble on heating.

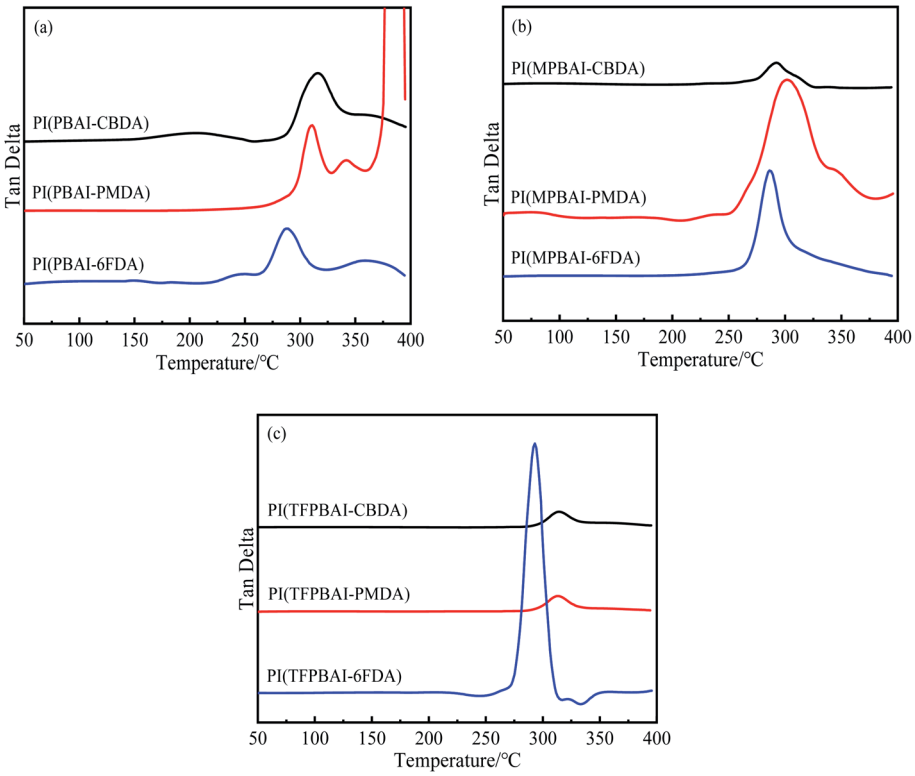

Fig. 3 Tan δ–T curves of triphenyl imidazole-containing polyimides (a) PIs based on PBAI, (b) PIs based on MPBAI, (c) PIs based on TFPBAI.

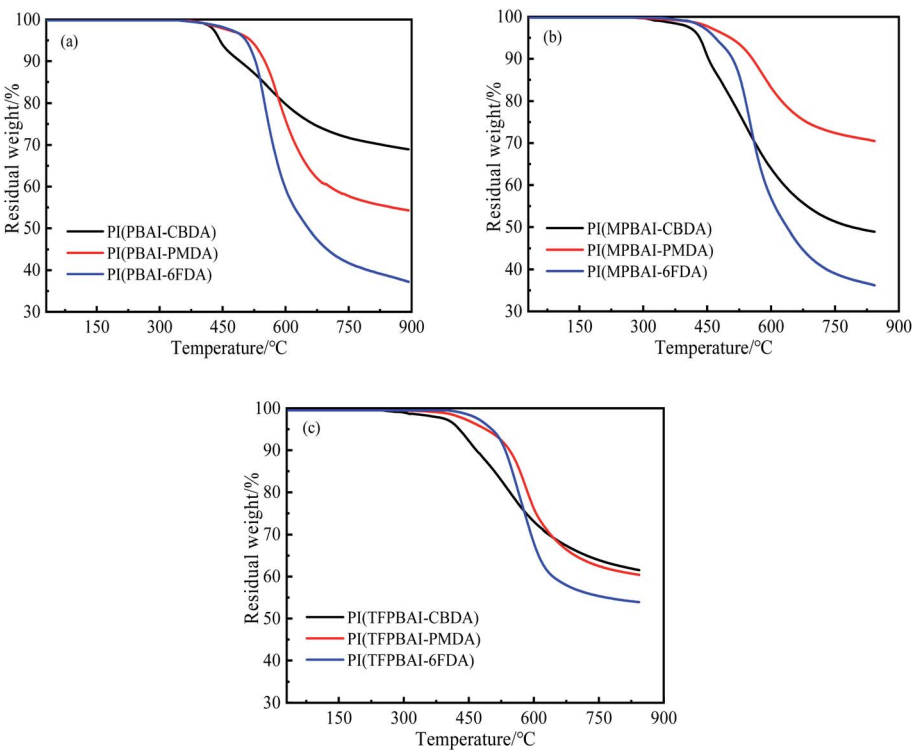

Fig. 4 TGA curves of triphenyl imidazole-containing polyimides (a) PIs based on PBAI, (b) PIs based on MPBAI, (c) PIs based on TFPBAI.

Table 2 Thermal and optical performance data of triphenyl imidazole-containing polyimides[a]

Samples	T_{d5} (°C)	T_{d10} (°C)	T_g (°C)	T_{500} (%)	λ_{cutoff} (nm)	Thickness (mm)
PI(PBAI-CBDA)	443.6	491.5	316	70.1	370	42
PI(PBAI-PMDA)	516.6	550.3	311	8.9	415	38
PI(PBAI-6FDA)	505.5	528.1	288	74.0	378	39
PI(MPBAI-CBDA)	432.3	452.9	292	71.0	405	37
PI(MPBAI-PMDA)	504.2	556.1	301	8.0	425	42
PI(MPBAI-6FDA)	468.9	509.5	286	63.4	410	35
PI(TFPBAI-CBDA)	428.0	467.6	314	76.1	380	37
PI(TFPBAI-PMDA)	489.6	544.2	315	19.3	410	30
PI(TFBTAI-6FDA)	503.3	534.3	293	75.9	390	46

[a] T_{d5}: the temperature at which the mass loss is 5%, T_{d10}: the temperature at which the weight loss is 10%, R_{800}: the residual weight at 800 °C, T_g: glass transition temperature tested by DMA, T_{500}: the transmittance at 500 nm, λ_{cutoff}: UV cutoff wavelength.

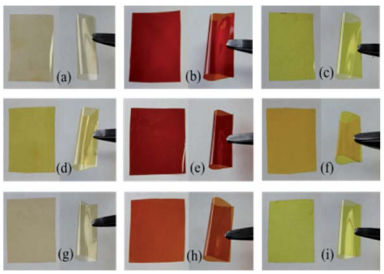

Fig. 5 Images of triphenyl imidazole-containing polyimide films (a) PI(PBAI-CBDA), (b) PI(PBAI-PMDA), (c) PI(PBAI-6FDA), (d) PI(MPBAI-CBDA), (e) PI(MPBAI-PMDA), (f) PI(MPBAI-6FDA), (g) PI(TFPBAI-CBDA), (h) PI(TFPBAI-PMDA), (i) PI(TFPBAI-6FDA).

rotation and motion ability of the molecular chains. The introduction of bulky and polar imidazole structures also facilitates the dissolution of polyimide in polar solvents. Thus, these polyimides show good processability.

3.4 Thermal properties

The data of thermal properties is a key index for the application of polymer materials. DMA and TGA were used to estimate the thermal properties of triphenyl imidazole-containing polyimides, the obtained tan δ–T curves and TGA curves are shown in Fig. 3 and 4 respectively, and the corresponding data is listed in Table 2. The glass transition temperature (T_g) of polymers could be affected by many factors, including the main chain structure, the steric hindrance of substituents and the

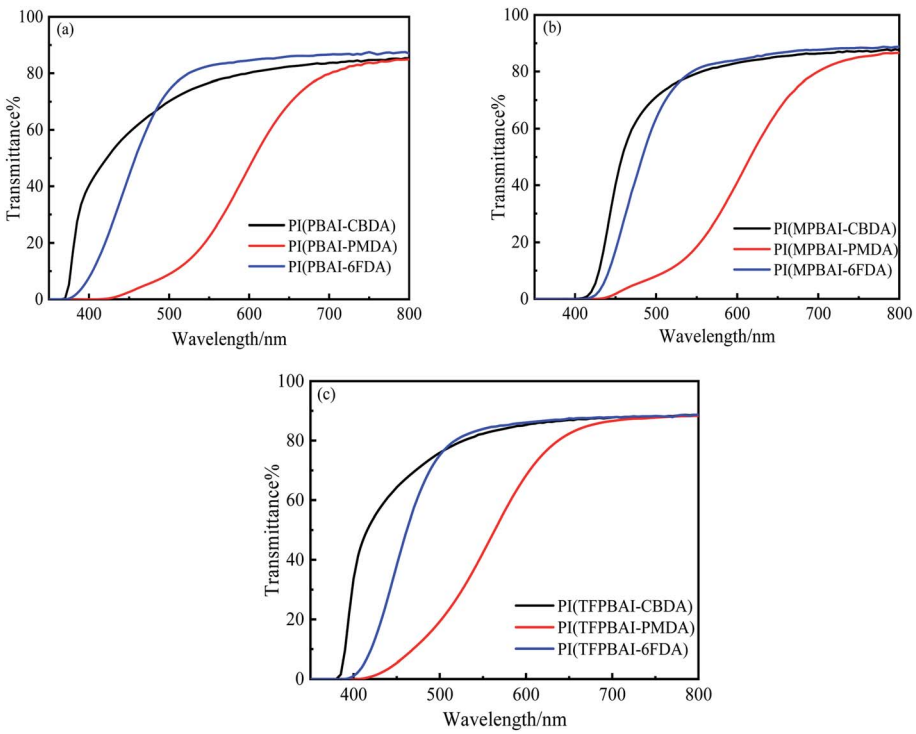

Fig. 6 UV-visible spectra of triphenyl imidazole-containing polyimide films (a) PIs based on PBAI, (b) PIs based on MPBAI, (c) PIs based on TFPBAI.

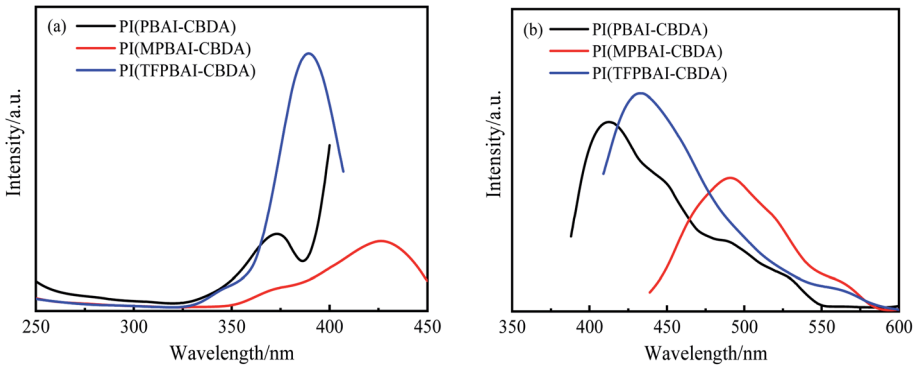

Fig. 7 Excitation–emission spectra of polyimide films based on dianhydride CBDA (a) excitation spectra, (b) emission spectra.

interaction between molecular chains. From Fig. 3, there is only one tan δ peak for each polyimide, corresponding to the T_g. These polyimides exhibit higher T_g values around 300 °C, indicating better thermal properties. By comparison, the polyimides based on PMDA and CBDA exhibit higher T_g than 6FDA-based PI, which is ascribed to the rigid structure of dianhydrides and strong interaction between molecular chains. The presence of hexafluoroisopropyl group could increase the molecular chain flexibility and reduce the interaction, resulting in T_g below 300 °C. Furthermore, the T_g values of TFPBAI-based polyimides are slightly higher, which is possibly due to the increase of $-CF_3$ steric hindrance and the restriction of the segment movement.

As shown in Fig. 4 and Table 2, the TGA curves of triphenyl imidazole-containing polyimides exhibit one main weightlessness process due to the pyrolysis of macromolecular backbone. The CBDA-based polyimides display lower thermal decomposition temperatures than the aromatic polyimides because of the poor stabilization of alicyclic structures. Due to the thermal instability of $-CH_3$ and $-CF_3$ substituent groups on the triphenyl imidazole, the thermal decomposition temperature T_{d5} and T_{d10} of PBAI-containing polyimides are relatively higher. In general, these triphenyl imidazole-containing polyimides exhibit excellent thermal stabilities, which could be applied in high temperature situations.

3.5 Optical properties

As we know, most of the conventional polyimide films always show considerable coloration ranging from pale yellow to deep brown due to the CTC effect, which greatly limits the optical application of the polyimides.[5] The images of triphenyl imidazole-containing polyimide films are given in Fig. 5, and the UV-visible spectra as well as the data of optical properties are shown in Fig. 6 and Table 2. It can be observed that the polyimide films containing CBDA dianhydride are light yellow with the shortest UV cut-off wavelength of 370 nm, and their optical transparency are above 70.1% at 500 nm. The introduction of alicyclic structure could weaken the conjugation of molecular chain and reduce the absorption of light. Because the bulky hexafluoroisopropyl groups enhance the distance between polymer backbones and decrease the formation of CTC, the 6FDA-based polyimide films exhibit light yellow with the shortest λ_{cutoff} of 378 nm and the highest transparency of 75.9% at 500 nm. However, the polyimides containing PMDA show deep brown color, which is mostly ascribed to the strong absorption of light induced by CTC effect and conjugated structures. Compared with the effect of R substituents on triphenyl imidazole, the polyimides containing TFPBAI have better optical properties, which are probably caused by the

Table 3 Fluorescence data of triphenyl imidazole-containing polyimide films[a]

PIs	λ_{max}^{ex} (nm)	λ_{max}^{em} (nm)	Φ_{PL} (%)
PI(PBAI-CBDA)	372	413	1.6
PI(MPBAI-CBDA)	426	489	3.3
PI(TFPBAI-CBDA)	389	434	2.7

[a] λ_{max}^{ex}: maximum excitation wavelength; λ_{max}^{em}: maximum emission wavelength; Φ_{PL}: fluorescence quantum yield.

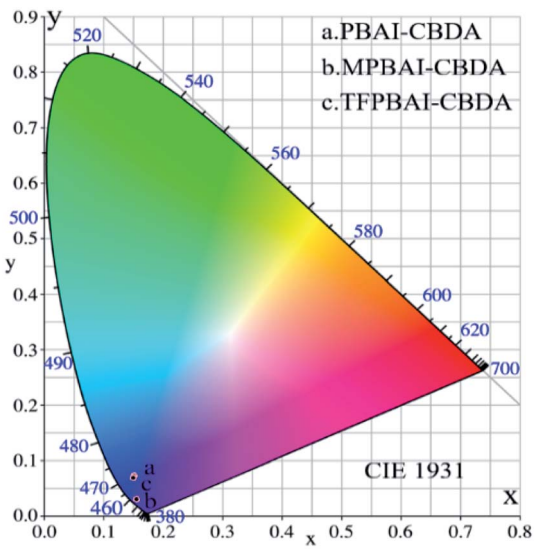

Fig. 8 CIE-1931 chromaticity diagrams of three PI films based on CBDA dianhydride.

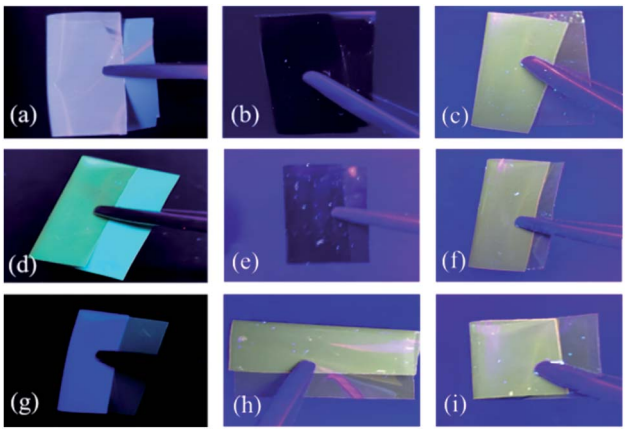

Fig. 9 Images of triphenyl imidazole-containing polyimide films under 365 nm ultraviolet light. (a) PI(PBAI-CBDA), (b) PI(PBAI-PMDA), (c) PI(PBAI-6FDA), (d) PI(MPBAI-CBDA), (e) PI(MPBAI-PMDA), (f) PI(MPBAI-6FDA), (g) PI(TFPBAI-CBDA), (h) PI(TFPBAI-PMDA), (i) PI(TFBTAI-6FDA).

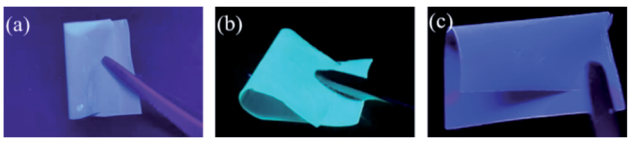

Fig. 10 Images of renewed polyimide films under 365 nm ultraviolet light (a) PI(PBAI-CBDA), (b) PI(MPBAI-CBDA), (c) PI(TFPBAI-CBDA).

steric hindrance effect of $-CF_3$ groups to further increase the distance between molecular chains and hinder the formation of CTC. Therefore, the optical properties of these polyimides could be easily adjusted by the dianhydrides and substituents on triphenyl imidazole of the diamines.

It is well known that the triphenyl imidazole structure has photoluminescence properties due to the conjugated and aromatic heterocyclic structures,[17] so it is expected that the polyimides containing triphenyl imidazole exhibit excellent photoluminescence properties. The fluorescence properties of three polyimide films with CBDA were tested, and the fluorescence quantum yields were obtained, as shown in Fig. 7 and Table 3. The polyimide films exhibit excitation maxima around 372–426 nm, coupled with fluorescence emission maxima about 413–489 nm. In the film state, the fluorescence quantum yields of these polyimides are less than 3.3%, which might be attributed to the strong fluorescence self-absorption effect. Comparatively speaking, PI(MPBAI-CBDA) and PI(TFPBAI-CBDA) exhibit higher fluorescence quantum yield than PI(PBAI-CBDA). Because the existence of $-CF_3$ or $-CH_3$ groups could hinder the close packing of molecular chains, which is helpful to enhance the intensity of fluorescence.

CIE was calculated from excitation spectra data of three polyimide films based on dianhydride CBDA, as shown in Fig. 8. The color coordinates of the emitted light of the three films are PI(PBAI-CBDA) ($x = 0.1503$, $y = 0.0737$), PI(MPBAI-CBDA) ($x = 0.1542$, $y = 0.0301$) and PI(TFPBAI-CBDA) ($x = 0.1496$, $y = 0.0698$). The CIE spectra and data show that the excitation lights of the three films are mainly in the blue range.

The photoluminescence images of triphenyl imidazole-containing polyimide films under 365 nm ultraviolet light in a dark room are shown in Fig. 9. It can be observed that the CBDA-based polyimide films show different photoluminescence effects. The PI(PBAI-CBDA) film exhibits purplish blue

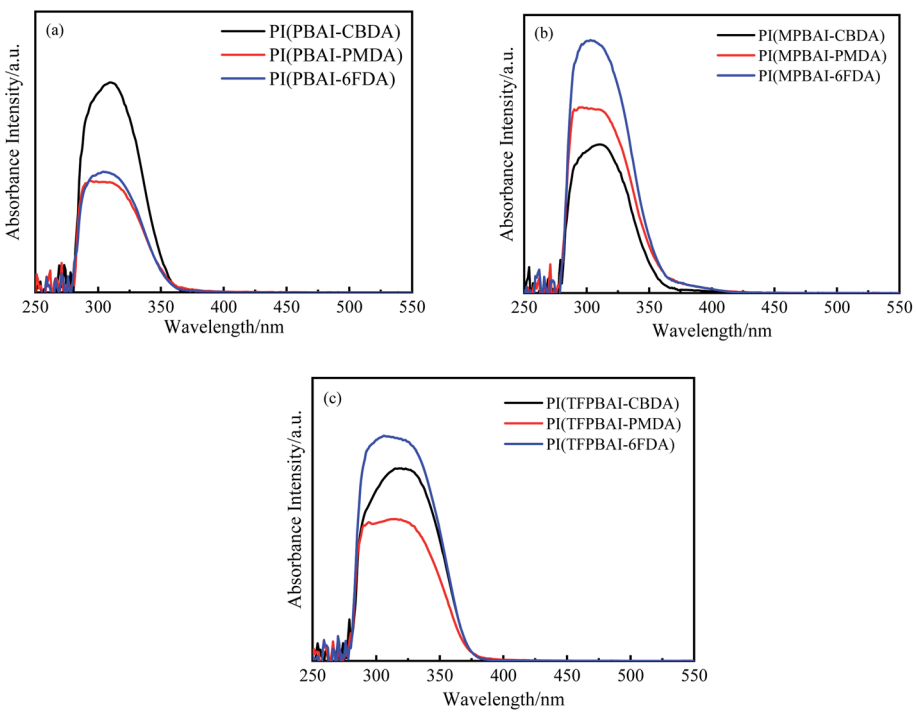

Fig. 11 Ultraviolet absorbance spectra of polyimides solution in DMAc (a) PIs based on PBAI, (b) PIs based on MPBAI, (c) PIs based on TFPBAI.

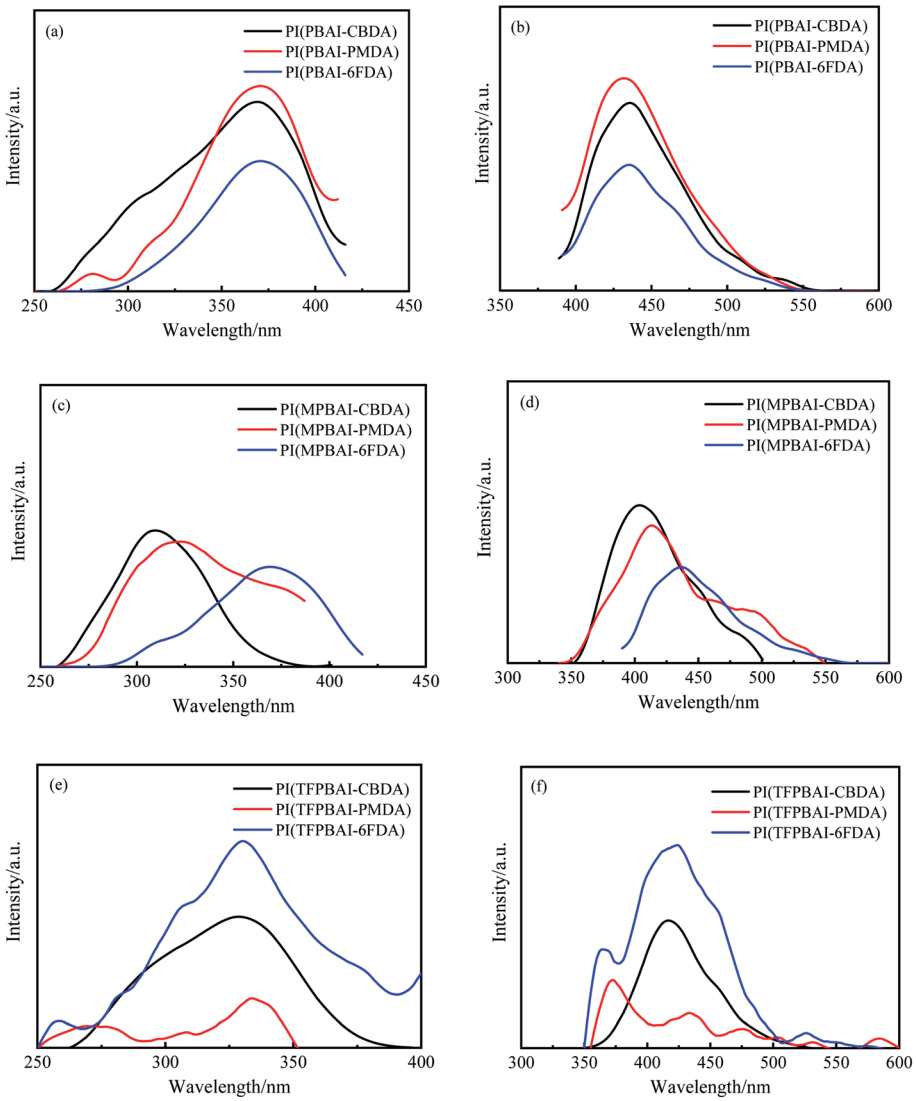

Fig. 12 Excitation–emission spectra of polyimide solution in DMAc (1×10^{-4} g L^{-1}) (a) excitation spectra of PIs with PBAI, (b) emission spectra of PIs with PBAI, (c) excitation spectra of PIs with MPBAI (d) emission spectra of PIs with MPBAI, (e) excitation spectra of PIs with TFPBAI, (f) emission spectra of PIs with TFPBAI.

fluorescence, the PI(MPBAI-CBDA) film displays light blue fluorescence, and the PI(TFPBAI-CBDA) film exhibits dark blue fluorescence, which are consistent with the chromaticity of polyimide films in Fig. 8. Meanwhile, the PI(PBAI-PMDA) and PI(MPBAI-PMDA) emit no obvious luminescence, and 6FDA-based polyimide and PI(TFPBAI-PMDA) have light yellow luminescence. According to the literatures,[49,50] the photoluminescence mechanism of polyimides includes the formation of locally excited (LE) state and charge transfer (CT) state in the typical donor–acceptor polyimide structures, and the influence for both of the states on their respective photoluminescence process. Here, the intrinsic fluorescence of polyimide films could be produced by triphenyl imidazole and the intra- and intermolecular charge transfer (CT) transition under the excitation of light. However, in the solid state, the aggregation state of molecular chains could strongly affect the CT transition and the photoluminescence performance of polyimide films. The introduction of ether linkage in the diamines could improve the flexibility of backbone and decrease the conjugation, which is benefit to weaken the CT transition between imidazole cycle (the electron donor structure) and trifluoromethyl-aryl-imide framework (the electron acceptor structure), limit the packing of chromogenic group and reduce the fluorescence quenching. For the polyimides based on CBDA, the non-coplanar and alicyclic dianhydride reduce the interaction between the molecular chains and conjugation, leading to weak CT effect. Because the polyimide films are not totally colorless but show yellowish colors, which maybe absorb the major part of blue fluorescence from the triphenyl imidazole moiety (*i.e.* self-absorption of the blue fluorescence). The energy transfer or self-absorption makes the polyimide films show different fluorescence properties. The planar characteristics of PMDA make the π–π^* interaction between the aromatic rings and the dipole–dipole interaction between the carbonyl groups of the imide ring strong, resulting in the close

Table 4 Fluorescence performance data of polyimide solutions[a]

Samples	λ_{max}^{abs} (nm)	λ_{onset}^{abs} (nm)	λ_{max}^{ex} (nm)	λ_{max}^{em} (nm)	Φ_{PL} (%)
PI(PBAI-CBDA)	310	377	369	436	15.4
PI(PBAI-PMDA)	311	429	371	432	13.5
PI(PBAI-6FDA)	320	406	371	435	12.1
PI(MPBAI-CBDA)	305	425	309	404	16.5
PI(MPBAI-PMDA)	304	450	323	413	13.3
PI(MPBAI-6FDA)	312	440	370	437	12.4
PI(TFPBAI-CBDA)	304	406	329	417	14.8
PI(TFPBAI-PMDA)	304	462	334	372	13.0
PI(TFBTAI-6FDA)	313	416	331	424	14.2

[a] λ_{max}^{abs}: maximum absorbance wavelength; λ_{onset}^{abs}: maximum absorption cut-off wavelength; λ_{max}^{ex}: maximum excitation wavelength; λ_{max}^{em}: maximum emission wavelength; Φ_{PL}: fluorescence quantum yield.

packing of molecular chains and the strong CT effect. The non-planar and bulky hexafluoroisopropyl groups from 6FDA could tend to make the polymer chains loose and weaken the CT effect.

Due to the excellent solubility of triphenyl imidazole-containting polyimides, the polyimide films based on CBDA were dissolved in the solvent DMAc at room temperature, and the films were prepared again (in Fig. 10). The regained films still emit obvious fluorescence like the original films, indicating the reusability and stability of the materials.

Fig. 11 shows the UV absorbance spectra of polyimide solutions in DMAc with a mass concentration of 1×10^{-4} g L^{-1}. The excitation–emission spectra of polyimide solutions are shown in Fig. 12, and the corresponding data are given in Table 4. All the polyimide solutions mostly emit similar blue fluorescence, the excitation wavelength maxima are between 309 and 371 nm, and the emission wavelength maxima are in the range from 372 to 437 nm. The CBDA-based polyimide solutions show higher quantum yield than the polyimides with 6FDA and PMDA. In the solution state, the polyimide molecular chains break away from the interaction between the molecular chains in the solid state and mainly present the state of a single molecular chain. The lowest energy one-electronic transitions of PMDA, CBDA, and 6FDA are all n–π* transitions, which emits almost no fluorescence. In contrast, triphenyl imidazole exhibits strong blue fluorescent emission. Thereby, the blue emission observed for the polyimide solutions could be explained by the fluorescence from the diamine moiety and intramolecular CT transition.

3.6 Electrochemical properties

Energy level is an important parameter for optoelectronic materials. The electrochemical performance of polyimide was tested using a three-electrode system, and the volt–ampere

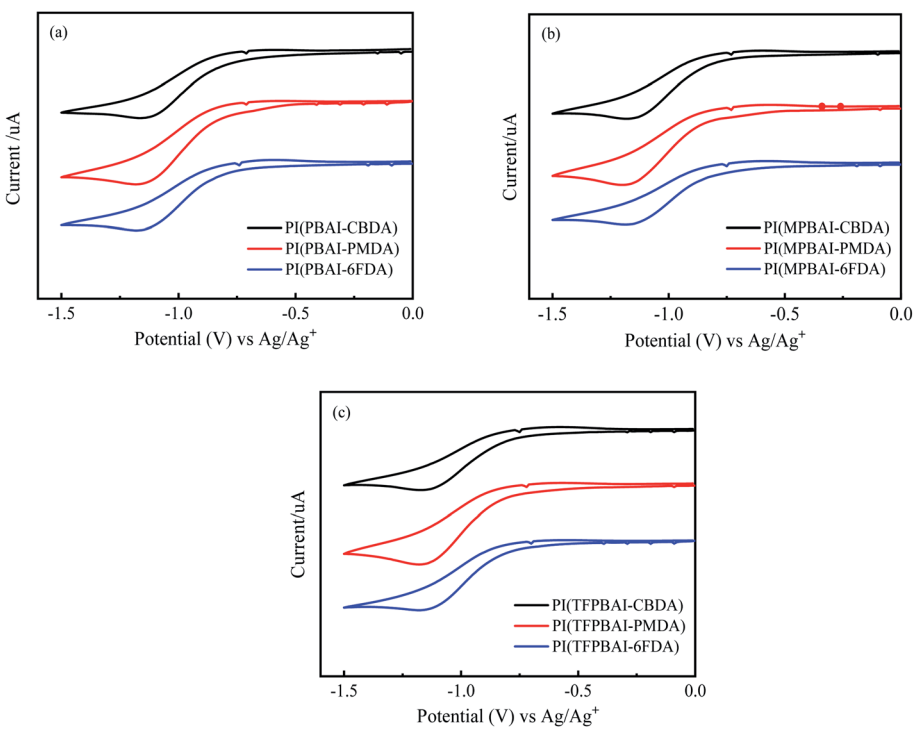

Fig. 13 Cyclic voltammograms of polyimides (a) PIs based on PBAI, (b) PIs based on MPBAI and (c) PIs based on TFPBAI.

Table 5 Electrochemical properties of polyimides[a]

Samples	λ_{onset}^{abs} (nm)	E_{onset}^{redox} (eV)	E_{HOMO} (eV)	E_{LUMO} (eV)	E_g^{opt} (eV)
PI(PBAI-CBDA)	377	−0.79	−6.90	−3.61	3.29
PI(PBAI-PMDA)	429	−0.80	−6.49	−3.60	2.89
PI(PBAI-6FDA)	406	−0.80	−6.65	−3.60	3.05
PI(MPBAI-CBDA)	425	−0.81	−6.51	−3.59	2.92
PI(MPBAI-PMDA)	450	−0.80	−6.35	−3.60	2.75
PI(MPBAI-6FDA)	440	−0.79	−6.43	−3.61	2.82
PI(TFPBAI-CBDA)	406	−0.78	−6.67	−3.62	3.05
PI(TFPBAI-PMDA)	462	−0.80	−6.28	−3.60	2.68
PI(TFBTAI-6FDA)	416	−0.79	−6.59	−3.61	2.98

[a] λ_{onset}^{abs}: maximum absorption cut-off wavelength; E_{onset}^{redox} (eV): reduction onset potential; E_{HOMO}: $E_{HOMO} = (E_{LUMO} - E_g^{opt})$ eV; E_{LUMO}: $E_{LUMO} = -E_{onset}^{redox}$ (eV) − 4.4 eV; E_g^{opt}: $E_g^{opt} = 1240/\lambda_{onset}^{abs}$ (nm) eV.

diagram is shown in Fig. 13. The LUMO level was calculated by using the intersection of the slopes of the line segments before and after the sudden change in the value of the volt–ampere curve as the reference value. The formula is as follows:

$$E_{LUMO} = -E_{onset}^{redox}\ (eV) - 4.4\ eV$$

The electrochemical data of the polyimides are shown in Table 5. It can be seen that the HOMO and LUMO data are almost close. The three diamine monomers with different R substituents have no significant effect on the HOMO and LUMO values.[51,52] The HOMO energy level of these polyimides was around −6.5 eV, and the corresponding LUMO energy level was about −3.60 eV, meeting the need for active semiconductors with a HOMO below −6.0 eV. For hole transport, the LUMO energy level needs to be close to or below −3.0 eV to achieve stable electron transport. Therefore, the triphenyl imidazole-containing polyimides are expected to be applied as functional materials in the photoelectric field in the future.

4. Conclusions

Three kinds of triphenyl imidazole-containing diamines PBAI, MPBAI, and TFPBAI were synthesized, and the corresponding polyimide films were prepared with CBDA, PMDA and 6FDA dianhydrides respectively, according to the two-step method. These polyimide films exhibited good thermal properties with higher T_g values around 300 °C, and the polyimides derived from CBDA and 6FDA showed better optical properties. All the polyimides displayed excellent solubility, especially in aprotic polar solvents, such as DMAc, DMF, DMSO and NMP. The polyimide films containing CBDA exhibited obvious photoluminescence properties, which emitted fluorescence in the blue range in the CIE 1931 spectrum. Meanwhile, all polyimide solutions showed similar blue fluorescence. Electrochemical tests showed that the HOMO values of these polyimides were all around −6.5 eV, the LUMO values were about −3.60 eV, and the energy gap difference was around 3.0 eV. Therefore, these triphenyl imidazole-containing polyimides will be expected to be used as functional materials for special optical and optoelectronic applications.

Conflicts of interest

There are no conflicts to declare.

Acknowledgements

This work was financially supported by the National Natural Science Foundation of China (grant number: 21878033), University of Science and Technology Liaoning Talent Project Grants (grant number: 601011507-17), Science and Technology Plan of Liaoning Province (grant number: 2020JH1/10100002).

References

1 R. Rajamanickam, P. Pichaimani and A. Muthukaruppan, *Polym. Bull.*, 2019, **76**, 387–407.
2 V. E. Ogbonna, A. P. I. Popoola, O. M. Popoola and S. O. Adeosun, *Polym. Bull.*, 2020, **77**, 1–33.
3 H. Araki, Y. Kiuchi, A. Shimada, H. Ogasawara and M. Tomikawa, *J. Photopolym. Sci. Technol.*, 2020, **33**, 165–170.
4 G. Vaganov, A. Didenko, E. Kova, E. Popova and I. Lasota, *J. Mater. Res.*, 2019, **34**, 1–8.
5 R. A. Dine-Hart and W. W. Wright, *Macromol. Chem. Phys.*, 1971, **143**, 189–206.
6 B. V. Kotov, T. A. Gordina, V. S. Voishchev, O. V. Kolninov and A. N. Pravednikov, *Polym. Sci.*, 1977, **19**, 711–716.
7 H. J. Yen and G. S. Liou, *Prog. Polym. Sci.*, 2019, **89**, 250–287.
8 Y. Zhuang, J. G. Seong and Y. M. Lee, *Prog. Polym. Sci.*, 2019, **92**, 35–88.
9 D. J. Liaw, K. L. Wang, Y. C. Huang, K. R. Lee, J. Y. Lai and C. S. Ha, *Prog. Polym. Sci.*, 2012, **37**, 907–974.
10 C. Y. Wang, B. Yu, C. R. Jiang, X. Y. Zhao, J. Li and Q. Ren, *Polym. Bull.*, 2020, **77**, 6509–6523.
11 Q. Wu, X. R. Ma, F. Zheng, X. M. Lu and Q. H. Lu, *Eur. Polym. J.*, 2019, **120**, 109235.
12 N. Mushtaq, G. Chen, L. R. Sidra and X. Fang, *RSC Adv.*, 2016, **6**, 25302–25310.
13 T. Matsumoto, H. Ozawa, T. Mizuta and S. Komatsu, *J. Photopolym. Sci. Technol.*, 2017, **30**, 133–137.
14 L. Li, J. Yin, Y. Sui, H. J. Xu, J. H. Fang, Z. K. Zhu and Z. G. Wang, *Polym. Adv. Technol.*, 2016, **81**, 1–35.

15 S. Bong, H. Yeo, B. C. Ku, M. Goh and N. H. You, *Macromol. Res.*, 2018, **26**, 85–91.
16 X. Que, Y. Yan, Z. Qiu and W. Yang, *J. Mater. Sci.*, 2016, **51**, 10833–10848.
17 H. Choi, I. S. Chung, K. Hong, E. P. Chan and Y. K. Sang, *Polymer*, 2008, **49**, 2644–2649.
18 K. Nakashima, Y. Fukuzaki, R. Nomura, R. Shimoda, Y. Nakamura, N. Kuroda, S. Akiyama and K. Irgum, *Dyes Pigm.*, 1998, **38**, 127–136.
19 K. Maeda, H. Ojima and T. Hayashi, *Bull. Chem. Soc. Jpn.*, 1965, **38**, 76–80.
20 N. Fridman, M. Kaftory and S. Speiser, *Sens. Actuators, B*, 2007, **126**, 107–115.
21 T. Yu, L. Liu, Z. Xie and Y. Ma, *Sci. China: Chem.*, 2015, **58**, 907–915.
22 T. Feczko and B. Voncina, *Curr. Org. Chem.*, 2013, **17**, 1771–1789.
23 X. Jiao, Y. Li, J. Niu, X. Xie, X. Wang and B. Tang, *Anal. Chem.*, 2018, **90**, 533–555.
24 T. Xia, J. Li, H. Cheng, C. Zhang and Y. Zhang, *Drug Dev. Res.*, 2015, **76**, 375–381.
25 S. C. Hsu, W. T. Whang and C. S. Chao, *Thin Solid Films*, 2007, **515**, 6943–6948.
26 Y. He, J. T. Li, J. Li, C. Zhu and J. Guo, *ACS Appl. Polym. Mater.*, 2019, **1**, 746–754.
27 E. F. Bernstein, H. W. Sarkas, P. Boland and D. Bouche, *J. Cosmet. Dermatol.*, 2020, **19**, 407–415.
28 J. Wakita, H. Sekino, K. Sakai, Y. Urano and S. Ando, *J. Phys. Chem. B*, 2009, **113**, 15212–15224.
29 M. Lian, F. Zheng, Q. Wu, X. M. Lu and Q. H. Lu, *Polym. Int.*, 2020, **69**, 93–99.
30 Z. Rafiee and M. Rasekh, *Polym. Adv. Technol.*, 2017, **28**, 533–540.
31 M. Ghaemy and R. Alizadeh, *Eur. Polym. J.*, 2009, **45**, 1681–1688.
32 M. Ghaemy, F. R. Berenjestanaki and M. Bazzar, *Des. Monomers Polym.*, 2014, **17**, 101–110.
33 A. Hariharan, S. Kumar, M. Alagar, K. Dinakaran and K. Subramanian, *Polym. Bull.*, 2018, **75**, 93–107.
34 X. F. Li, Y. J. Liu, H. B. Chen and H. M. Li, *Eur. Polym. J.*, 2019, **121**, 109347.
35 M. Ghaemy and F. R. Berenjestanaki, *J. Fluorine Chem.*, 2012, **144**, 86–93.
36 M. Ghaemy and S. M. A. Nasab, *Polym. Adv. Technol.*, 2011, **22**, 2311–2318.
37 F. Akutsu, M. Inoki, M. Sawano, Y. Kasashima and M. Miura, *Polymer*, 1998, **39**, 6093–6098.
38 J. C. Jung and S. B. Park, *Polym. Bull.*, 1995, **35**, 423–430.
39 H. Choi, I. S. Chung, K. Hong, C. E. Park and S. Y. Kim, *Polymer*, 2008, **49**, 2644–2649.
40 Z. Rafiee and M. Mohagheghnezhad, *Polym. Bull.*, 2019, **6**, 3857–3877.
41 C. K. Chen, Y. C. Lin, S. Miyane, S. Ando and W. C. Chen, *ACS Appl. Polym. Mater.*, 2020, **2**, 3422–3432.
42 E. D. Wachsman and C. W. Frank, *Polymer*, 1988, **29**, 1191–1197.
43 M. Hasegawa, I. Mita, M. Kochi and R. Yokota, *Polymer*, 1991, **32**, 3225–3232.
44 T. T. Yang, Z. X. Zhou, Z. Yi, S. W. Liu, Z. G. Chi and J. R. Xu, *Acta Polym. Sin.*, 2016, **3**, 411–428.
45 Z. Zhou, Y. Zhang, S. W. Liu, Z. Chi, X. Chen and J. Xu, *J. Mater. Chem. C*, 2016, **44**, 10509–10517.
46 A. Ghosh, S. Banerjee and B. Voit, *Aromatic Hyperbranched Polymers: Synthesis and Application*, Springer International Publishing, 2014, pp. 27–124.
47 P. Liu, P. Zhang, D. Cao, L. Gan and Y. Li, *J. Mol. Struct.*, 2013, **1050**, 51–158.
48 L. Qu, L. Tang, R. Bei, J. Zhao, Z. Chi, S. W. Liu, X. Chen, M. P. Aldred, Y. Zhang and J. Xu, *ACS Appl. Mater. Interfaces*, 2018, **10**, 11430–11435.
49 L. J. Qu, L. S. Tang, S. W. Liu, Z. G. Chi, X. D. Chen, Y. Zhang and J. R. Xu, *Acta Polym. Sin.*, 2018, **11**, 1430–1441.
50 T. T. Yang, Z. X. Zhou, Y. Zhang, S. W. Liu, Z. G. Chi and J. R. Xu, *Acta Polym. Sin.*, 2017, **3**, 411–428.
51 C. J. Chen, J. Hung, H. J. Yen, Y. C. Hu and G. S. Liou, *J. Mater. Chem. C*, 2013, **1**, 7623–7634.
52 A. Hariharan, S. Kumar, M. Alagar, K. Dinakaran and K. Subramanian, *Polym. Bull.*, 2018, **75**, 93–107.